ACS Catalysis

Research Article

pubs.acs.org/acscatalysis

Are Solvent and Dispersion Effects Crucial in Olefin Polymerization DFT Calculations? Some Insights from Propylene Coordination and Insertion Reactions with Group 3 and 4 Metallocenes

Ludovic Castro,[†] Evgueni Kirillov,[‡] Olivier Miserque,[§] Alexandre Welle,[§] Luc Haspeslagh,[∥] Jean-François Carpentier,[‡] and Laurent Maron*[,†]

[†]LPCNO, UMR 5215, Université de Toulouse, INSA, UPS and CNRS, 135 avenue de Rangueil, F-31077 Toulouse, France

[‡]Organometallics, Materials and Catalysis laboratories, UMR 6226 Institut des Sciences Chimiques de Rennes, CNRS-Université de Rennes 1, F-35042 Rennes, France

[§]Total Petrochemicals Research, Zone Industrielle C, B-7181 Feluy, Belgium

[∥]Total S.A., Direction scientifique, 24 Cours Michelet, F-92069 Paris La Défense Cedex, France

Supporting Information

ABSTRACT: The primary insertion (or 1,2-insertion) of propylene into $(C_5Me_5)_2YCH_2CH_2CH(Me)_2$, as well as the primary and secondary (or 2,1) insertions of propylene into the activated *ansa*-zirconocene complex $[\{Ph(H)C\text{-}(3,6\text{-}t\text{Bu}_2\text{Flu})(3\text{-}t\text{Bu-}5\text{-Me-}C_5H_2)\}ZrMe]^+$ were calculated with several DFT methods to find the most adequate methodology for the computation of metallocene-catalyzed olefin polymerization reactions. For the yttrium system, both solvent corrections and dispersion corrections are needed to determine energies of coordination and activation barriers in agreement with experimental data. Dispersion corrections were included directly via the use of specific functionals like B97D and M06 or were added as empirical corrections (GD3BJ) to the B3PW91 calculations. For the zirconocene system, the best method is a combination of B3PW91 with solvent corrections incorporated with the SMD continuum model. The dispersion corrections, included via both GD3BJ and M06, tend to overestimate the stabilization of the adducts because of the high steric bulk of the zirconocene system. The addition of dispersion corrections shifts the energy profiles toward lower values but does not affect the relative activation barriers. Implementation of entropy corrections counterbalances almost perfectly the dispersion corrections. The same observations arise from the study of the C−H activations of propylene induced by the zirconocene complex.

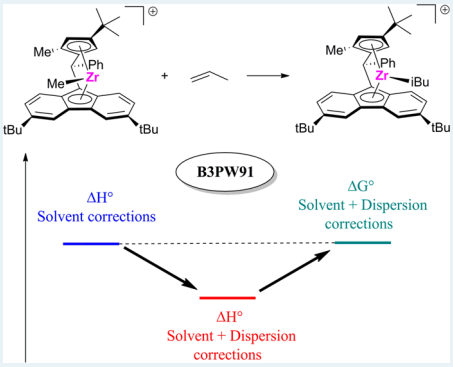

KEYWORDS: *DFT, dispersion correction, solvent effects, entropy correction, olefin polymerization*

INTRODUCTION

Carbon-linked multisubstituted fluorenyl-cyclopentadienyl (hereafter denoted as Flu and Cp, respectively) group 4 metal complexes have attracted considerable attention from both academic and industrial communities because of their remarkably high catalytic activity and stereoselectivity in polymerization of propylene.[1,2] Following the seminal report of the formation of syndiotactic polypropylene with the C_s-symmetric metallocene $\{Me_2C\text{-}(C_5H_4)(C_{13}H_8)\}ZrCl_2$ by Ewen et al.,[3] several groups have prepared structural variants of this parent complex thanks to its highly tunable ligand platform. Polypropylenes generated by some of these variants were no longer syndiotactic but displayed alternative tacticities depending on the nature of the substituents on the Cp ligands.[3b,4,5] For instance, some of us recently reported several structural variations of the parent zirconocene, with monosubstituted one-carbon linkers.[6] Among those, the C_1-symmetric precursor **1** (Figure 1), when activated by MAO (MAO = methylaluminoxane), displayed a superior catalytic activity and provided a high level of stereocontrol for the production of highly isotactic polypropylene.[6a]

In the last decades, computational chemistry has become a very powerful tool aimed at assisting the experiments. For example, computational studies can help to understand the steric and electronic properties of organometallic catalysts, rationalize mechanistic pathways and, therefore, give some insights in order to optimize the structures and improve performances of existing families of catalysts. Lately, these methods have become precise enough to compute and pinpoint subtle effects like the stereoselectivity and regioselectivity of the catalysts and thus to predict the tacticity of the formed polymers.[7] Density Functional Theory (DFT) is the most prominent method used in the literature due to its very satisfying compromise between calculation cost and robustness.

Received: October 24, 2014
Revised: November 28, 2014
Published: December 3, 2014

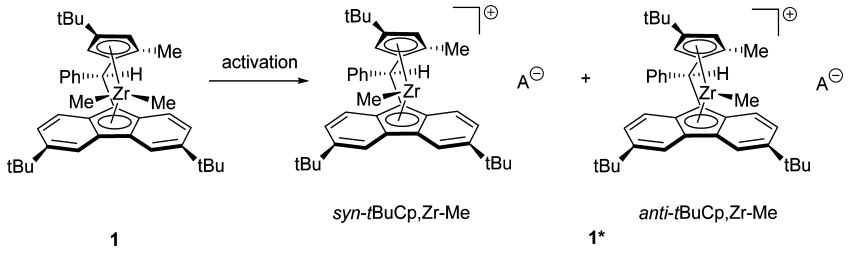

Figure 1. Zirconocene precursor **1** and its respective activated species **1*** (a "simplified" model used when counteranion A^- is excluded from calculations).

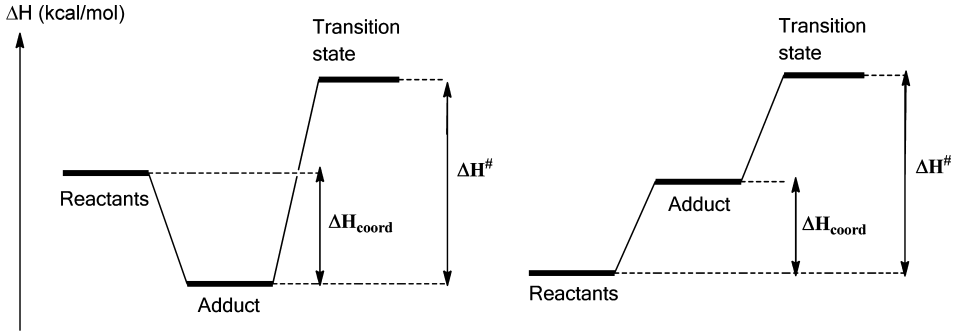

Figure 2. Definition of $\Delta H^{\#}$ depending on the sign of ΔH_{coord}.

Hybrid functionals (e.g., B3PW91) as well as GGA functionals (e.g., BP86) are commonly used for the study of metal-mediated polymerization processes.[8,9] However, although many DFT studies have been performed to assess individual metallocene catalyst systems,[8−10] the literature still lacks methodological studies.

Hence, in this article, we wish to compare several DFT methodologies for the insertion of propylene into the activated version of complex **1** (see complex **1*** in Figure 1). Complex **1*** is monocationic, and it is usually assumed that the counterion $[MAO]^-$ is weakly bonded with the Zr center. This anion can play a major effect in the determination of the reaction rate because its extraction from the catalyst center may cost a large amount of energy. However, it is reasonable to assume that the magnitude of this effect should be the same for all different types of insertions. The MAO molecule must be included when computing absolute rates of polymerization but not for the prediction of stereoselectivity and regioselectivity. Ziegler and Razavi used to treat this effect in their theoretical studies by using QM/MM calculations.[7,8] In our case, we wanted to compare different methodologies and gain some insights about the stereoselectivity and the regioselectivity of the catalyst; so the MAO molecule was not simulated and the only studied reactant is cation **1***. By testing different methods, we especially aimed at systematically scrutinizing the impact of both solvent (included by means of continuum model SMD)[11] and dispersion effects, which was included via three different ways: the GGA functional B97D,[12] the meta-GGA functional M06[13] and the semiempirical dispersion correction GD3BJ[14] in addition with B3PW91.[15]

The first part of this study addresses a comparison between the experimental energetic data of the primary insertion (or 1,2-insertion) of propylene into the yttrium metallocene complex $(C_5Me_5)_2YCH_2CH_2CH(Me)_2$ (**2**)[16] and the respective data calculated with different methods. The neutral Y(III) complex is an isoelectronic model for a putative Zr(IV) cationic species of the type $[(C_5Me_5)_2ZrCH_2CH_2CH(Me)_2]^+$ because, to our knowledge, no relevant energetic data has been reported experimentally for such zirconocene complexes. Then, in a second part, the best methods were evaluated on the primary and secondary (or 2,1) insertions of propylene into the Zr−alkyl bond of complex **1*** and on various C−H activations of propylene. The results of these studies show that the dispersion correction calculated with GD3BJ is clearly overestimated for the insertion of propylene into the Zr−alkyl bond of **1***, although the optimization of transition states is more time-consuming when this correction is included.

COMPUTATIONAL DETAILS

All calculations were carried out with the Gaussian 09 suite of programs.[17] Yttrium and zirconium atoms were treated with their respective very small core Stuttgart−Dresden effective core potentials associated with their adapted basis sets and additional *f* and *g* polarization functions.[18] Carbon and hydrogen atoms were described with a 6-31G(d,p) double-ζ basis set.[19] The majority of the calculations were carried out at the DFT level of theory with the hybrid functional B3PW91,[15] while others were performed with the GGA functional B97D[12] and the meta-hybrid GGA functional M06[13] in order to take into account the dispersion effects. Solvation energies were evaluated by a self-consistent reaction field (SCRF) approach based on accurate numerical solutions of the Poisson−Boltzmann equation by using the SMD solvation model.[11] Methylcyclohexane and toluene were used as solvents for the yttrium and the zirconium systems, respectively. Dispersion corrections were also treated with the D3 version of Grimme's dispersion with Becke−Johnson damping (GD3BJ).[14] All geometries were optimized without any symmetry restriction, and the nature of the extrema was verified by analytical frequency calculations. The calculation of electronic energies, enthalpies, and Gibbs free energies of the extrema of the potential energy surface (minima and transition states) were performed at the same level of theory as the geometry optimizations. Enthalpies and Gibbs free energies were

dx.doi.org/10.1021/cs5016436 | ACS Catal. 2015, 5, 416−425

obtained at T = 298 K within the harmonic approximation. In order to compare experimental and calculated activation barriers for the yttrium system, $\Delta H^{\#}$ was calculated instead of $\Delta G^{\#}$ because of the well-known erroneous computational description of the variation of entropy for a reaction where two reactants give only one product in solution.[20] The way how $\Delta H^{\#}$ was calculated is presented in Figure 2. IRC calculations were performed to confirm the connections of the optimized transition states. The electronic charges (at the DFT level) were computed using the natural population analysis (NPA).[21]

RESULTS AND DISCUSSION

1. Yttrium System. In order to compare different methodologies, we first focused on a very simple insertion reaction whose coordination energies and activation energies were determined experimentally.[16] The reaction between complex **2** and propylene takes places at T = −130 °C in a 1:1 mixture of methylcyclohexane-d_{14} and pentane-d_{12}. The propylene molecule inserts into the Y−CH_2 bond in a primary fashion to form the corresponding insertion product $(C_5Me_5)_2YCH_2CH(Me)CH_2CH_2CH(Me)_2$ (Figure 3). The

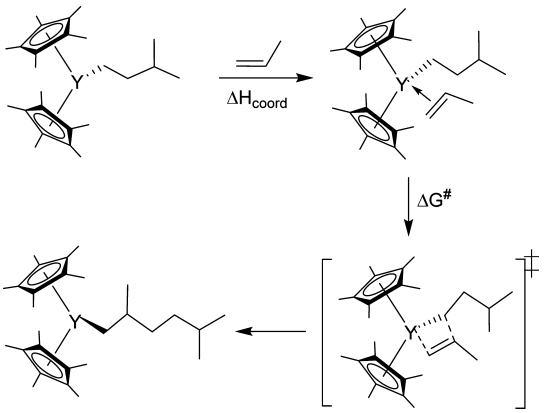

Figure 3. Primary insertion of propylene into yttrium complex **2**.

authors showed by ^{1}H NMR spectroscopy that there is a rapid equilibrium between free and bound propylene, and hence the variation of enthalpy related to propylene coordination was found to be ΔH_{coord} = −4.5(3) kcal/mol thanks to measurements at various temperatures (between −150 °C and −100 °C). Moreover, the activation energy of the primary insertion of propylene into **2** was found to be $\Delta G^{\#}$ (−100 °C) = +11.5(2) kcal/mol.

As summarized in Table 1, the geometries of the propylene molecule, complex **2**, the adduct and the transition state of the primary insertion were all optimized with 7 different methods (**A**−**G**). Methods **A**, **B**, and **C** include the hybrid B3PW91 functional which does not incorporate any dispersion effects. Methods **A**, **D**, and **F** assume calculations in the gas phase, whereas methods **B**, **E**, and **G** implement the SMD continuum model treating the solvent effects. Method **C** adds the dispersion effects by means of the empirical correction GD3BJ. Methods **D** and **E** include the GGA functional B97D, whereas methods **F** and **G** include the meta-GGA functional M06. Both of these functionals incorporate dispersion effects. These 7 different methodologies present an exhaustive range of combinations of the relevant effects that appear in a molecular system in solution.

The transition state structure of the reaction is a typical π-metathesis transition state (Figure 3).[22] The value of ΔH_{coord} calculated using method **A** is +2.5 kcal/mol. This shows that the coordination complex is less stable than the separated reactants, which is in disagreement with the experimental data. On the other hand, the activation barrier is calculated to be +9.5 kcal/mol, which is very close to the experimental value. When the solvation model SMD is implemented (method **B**), the propylene molecule does not remain coordinated to Y during the optimization but prefers to leave the coordination sphere instead. Indeed, the SMD model tends to stabilize more the separated reactants because stabilizing interactions between both complex **2** and propylene with the surrounding solvent have to be broken for formation of the adduct. As a result, the adduct calculated using this model should be even less stable than that from method **A**. That is the reason why the propylene molecule prefers to leave the coordination sphere. For the same reason, the calculated activation barrier is higher than for method **A**. However, if the dispersion effects are added with GD3BJ (method **C**), a reversed effect happens. When the propylene molecule coordinates to complex **2**, stabilizing intramolecular London forces appear and eventually stabilize the adduct (−6.3 kcal/mol, that is quite close to the experimental value). For the same reason, the calculated activation barrier is also smaller than the experimental one by 4 kcal/mol, which is still within the systematic error of the DFT method (2−3 kcal/mol).[23] For methods **D** and **E**, the dispersion effects are already included in the functional B97D, so the computed adducts are very stable. In the gaseous phase (method **D**), the ΔH_{coord} value is equal to −11.8 kcal/mol, which is significantly more negative than the experimental value. The solvation model SMD (method **E**) helps to

Table 1. Coordination and Activation Enthalpies (kcal/mol) of the Primary Insertion of Propylene into $(C_5Me_5)_2YCH_2CH_2CH(Me)_2$, Calculated with Different DFT Methods[a]

label	method	ΔH_{coord}	$\Delta H^{\#}$	RMS[b]
A	B3PW91/6-31G**/SDD	+2.5	+9.5	5.1
B	B3PW91/6-31G**/SDD/SMD	no stable adduct	+15.8	4.3[c]
C	B3PW91/6-31G**/SDD/SMD/GD3BJ	−6.3	+7.3	3.2
D	B97D/6-31G**/SDD	−11.8	+8.0	3.7
E	B97D/6-31G**/SDD/SMD	−8.5	+9.4	3.2
F	M06/6-31G**/SDD	−8.3	+6.4	4.5
G	M06/6-31G**/SDD/SMD	−6.1	+8.0	2.8
	experiments[16]	−4.5	+11.5 ($\Delta G^{\#}$)	

[a] $\Delta H^{\#}$ is calculated with respect to the coordination complex when ΔH_{coord} is negative and with respect to the separated reactants when ΔH_{coord} is positive or when no adduct is present (see Figure 2). [b] $RMS = ((\Sigma(E_{exp} - E_{calc})^2/2)^{0.5}$. [c] Calculated from the value of $\Delta H^{\#}$.

dx.doi.org/10.1021/cs5016436 | ACS Catal. 2015, 5, 416−425

counterbalance the effect of the dispersion but the calculated ΔH_{coord} value appears still too negative; this suggests that the dispersion correction of B97D is likely overestimated. A similar effect has been recently reported by Reiher et al.[24] On the other hand, the calculated activation barriers are close to the experimental ones. For methods **F** and **G**, the dispersion effects are already partially included in the meta-GGA functional M06, so the calculated ΔH_{coord} values are negative. When the solvent is included (method **G**), ΔH_{coord} is really close to the experimental value, the same as for method **C**. The calculated activation barrier is smaller than the experimental one, but the difference (3.5 kcal/mol) is still within the systematic error of DFT.

In conclusion, no method reproduces impeccably the experimentally determined ΔH_{coord} and $\Delta G^{\#}$ values but the results of methods **C**, **E**, and **G** seem to be quite reasonable. These are the three principal methods, which include at the same time solvation and dispersion effects.

2. Zirconocenium System. In order to study the insertions of propylene with cationic complex **1***, we have proceeded stepwise using methods **A**, **B**, and **C** to notice the differential effects of these three methods. Method **G** has also been tested only for the insertion reactions. Hereafter, complex **1*** is denoted [Zr]-Me in the figures, where [Zr] stands for the cationic moiety, including the zirconium center and the Ph(H)C-bridged substituted Cp-Flu ligand.

Two main types of insertions of propylene are possible into **1***: the primary and secondary insertions, which lead to *iso*-butyl and *sec*-butyl products, respectively (Figure 4). However,

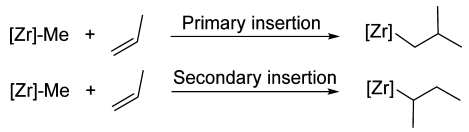

Figure 4. Primary and secondary insertions of propylene into **1***.

eight different insertions have to be considered, as depicted in Figure 5. Indeed, complex **1*** can exist in two different configurations: the [Zr]−methyl group can use the coordination site in *anti* or in *syn* position with respect to the *t*Bu group of the Cp ligand (these two possibilities are denoted as A and S hereafter). Moreover, the propylene molecule can insert into the Zr−CH_3 bond via either the *re* or *si* face. For a primary insertion, both *re* and *si* insertions lead to the same product (i.e., the *iso*-butyl complex), which does not contain any asymmetric carbon in the Zr−alkyl group. On the other hand, for a secondary insertion, *R* or *S* chiral centers are generated in the final *sec*-butyl product, depending on which face (*re* or *si*) coordination took place. Hereafter, the general notation for the insertions will be for example A-pr-*si* for the primary insertion *si* into the *anti* configuration of complex **1***. It is also noteworthy that for an insertion into the *anti* conformation, propylene inserts at the more crowded site of the catalyst and that the resulting product will use in turn the *syn* coordination site for the forthcoming insertion step. Similarly, for the insertion into the *syn* conformation of **1***, propylene inserts at the less crowded site and the resulting product will use the *anti* coordination site.

The optimized structures of both *anti* and *syn* configurations of the reactant **1*** are presented in Figure 6. For the *syn* configuration, the Zr−methyl group lies on the more crowded coordination site having the bulky *t*Bu substituent on the Cp ligand. A small deformation of the Flu ligand appears to form a small stabilizing interaction between the aromatic six-membered ring and Zr at the less crowded side of the catalyst. It is however not enough to counterbalance the slight steric repulsion between the Zr−methyl group and the *t*Bu substituent since the *syn* configuration is less stable by +4.4, +2.5 and +2.7 kcal/mol (computed with methods **A**, **B**, and **C**, respectively) with respect to the *anti* configuration.

Energetic data of the four possible insertions starting from the *anti* configuration have been computed (Table 2). For a given method, it is noteworthy that the adducts for the primary insertions are more stable as compared to those for the yttrium system (for example, for method **A**, −10 kcal/mol versus +2.5 kcal/mol in the case of yttrium). Yet, for method **B**, a stable adduct was localized, whereas there was no stable analogue optimized for the yttrium system. This suggests that complex **1*** is a better Lewis acid than complex **2**. This most likely stems from its cationic nature/positive charge as well as from the fact that it is an *ansa*-metallocene, hence with a more open coordination sphere. Indeed the Cp−Zr−Flu angle in complex **1*** is 121° whereas the Cp−Y−Cp angle in complex **2** is 139°, when calculated with method **A**. As mentioned before, the SMD component tends to destabilize the formation of the

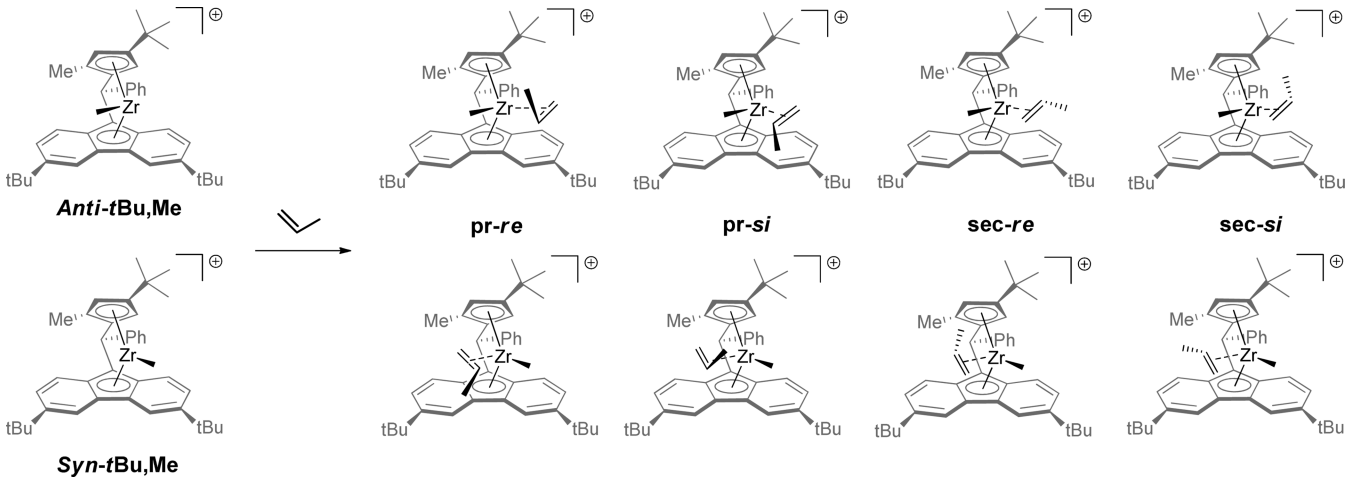

Figure 5. Eight possible adducts for the coordination/insertion of propylene into the Zr−CH_3 bond of **1***.

dx.doi.org/10.1021/cs5016436 | ACS Catal. 2015, 5, 416−425

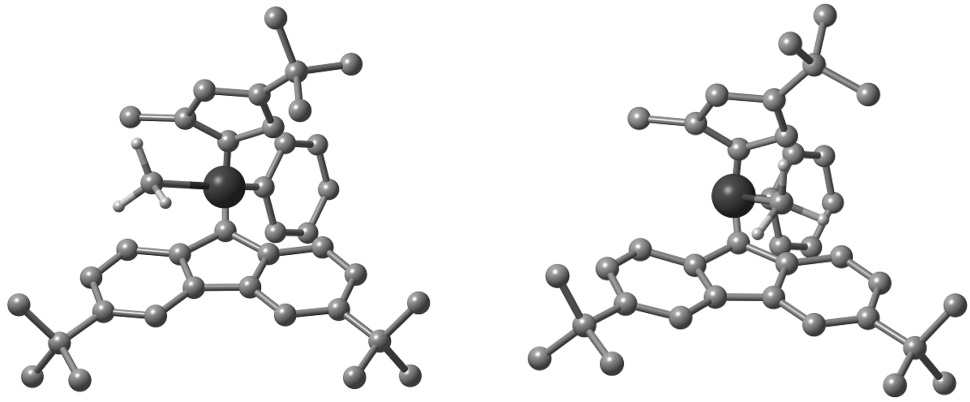

Figure 6. Optimized structures of the *anti* (left) and *syn* (right) configurations of complex **1*** with method **C**. Hydrogen atoms except those of the Zr−Me group have been omitted for clarity.

Table 2. Energetic Data Calculated for the Insertion Reactions between Complex 1* and a Propylene Molecule[a]

reaction		ΔH (**A**)	ΔH (**B**)	ΔH (**C**)	ΔG (**C**)
A-pr-*re*	adduct	−10.4	−3.1	−15.7	−2.6
	TS	+8.7	+11.7	+11.2	+12.0
	product	−7.8	−11.5	−9.5	−8.6
A-pr-*si*	adduct	−10.1	−3.4	−15.0	−2.3
	TS	+8.5	+11.9	+9.9	+12.4
	product	−8.1	−11.3	−10.2	−8.9
A-sec-*re*	adduct	−4.2	+0.2	−11.2	+1.9
	TS	+11.8	+15.9	+13.9	+16.0
	product	−5.6	−4.2	−5.7	−3.0
A-sec-*si*	adduct	−6.1	−0.6	−13.3	−1.9
	TS	+16.0	+19.5	+19.5	+22.3
	product	−1.0	−0.9	−0.8	+1.6
S-pr-*re*	adduct	−11.8	−4.3	−16.5	−3.4
	TS	+8.6	+11.3	+8.5	+9.6
	product	−8.9	−13.5	−12.7	−12.0
S-pr-*si*	adduct	−11.0	−3.6	−16.7	−4.4
	TS	+7.9	+10.8	+9.1	+11.3
	product	−9.7	−14.1	−12.5	−11.0
S-sec-*re*	adduct	−9.7	−2.6	−15.1	−1.8
	TS	+11.0	+14.3	+11.2	+11.2
	product	−5.5	−7.0	−8.8	−8.4
S-sec-*si*	adduct	−11.3	−3.2	−15.6	−3.8
	TS	+17.2	+18.3	+16.4	+18.2
	product	+1.4	−2.7	−2.5	+1.0

[a]All values are given in kcal/mol. The activation energies and the energies of reaction are given with respect to the corresponding adducts.

olefin adduct (from −10.4 to −3.1 kcal/mol for A-pr-*re*), while the GD3BJ component tends to significantly stabilize the adduct (from −3.1 to −15.7 kcal/mol for A-pr-*re*). The dispersion effects of GD3BJ again tend to overestimate the adduct stabilization, whereas there may be an equilibrium between free and coordinated propylene in solution for this kind of zirconocene complexes. The addition of entropic contributions within method **C** destabilizes the olefin adduct again (from −15.7 to −2.6 kcal/mol for A-pr-*re*). Indeed, the formation of an adduct from two reactants leads to a loss of disorder, i.e. to a loss of entropy.

For all methods, however, the relative activation barriers and the energies of reaction are basically the same (respectively around +11 and −10 kcal/mol for A-pr-*re*). It is thus noticeable that the solvent, the dispersion and the entropy contributions all induce only variations of the energy of the adduct with respect to the separated reactants; on the other hand, the relative activation energies and enthalpies of reaction do not vary. These three effects thus only shift the overall energy profiles of the reactions. In particular, it is noteworthy that the energies calculated with ΔH (**B**) and ΔG (**C**) are basically the same, which suggests that the dispersion and entropy effects actually compensate each other. These global observations are true for the four insertion reactions. This result is not really unique since, in a recent study, Kefalidis et al.[25] found the same trend in reactivity of magnesium complexes.

Because relative activation barriers are not really dependent on the method used, electronic and geometrical parameters at the transition states level were expected not to change significantly. In order to actually probe this, relevant structural parameters and electronic NPA charges were computed (Figure

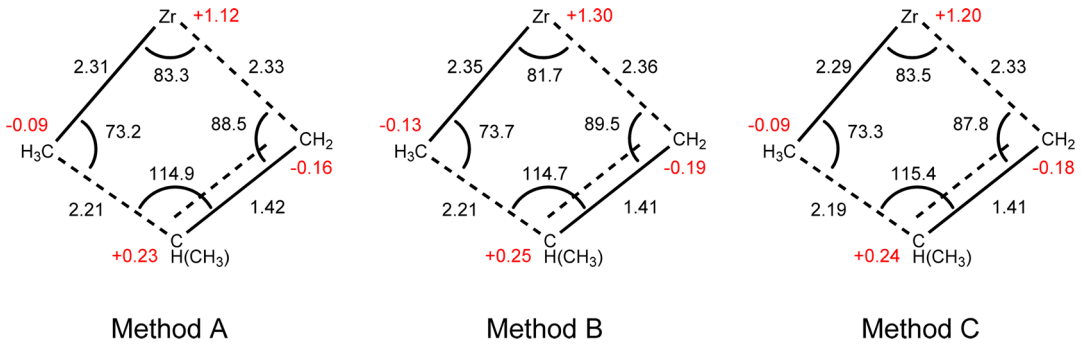

Figure 7. Selected geometrical parameters and NPA charges of the optimized structures of the A-pr-*si* transition state for the three different methods.

dx.doi.org/10.1021/cs5016436 | *ACS Catal.* 2015, 5, 416−425

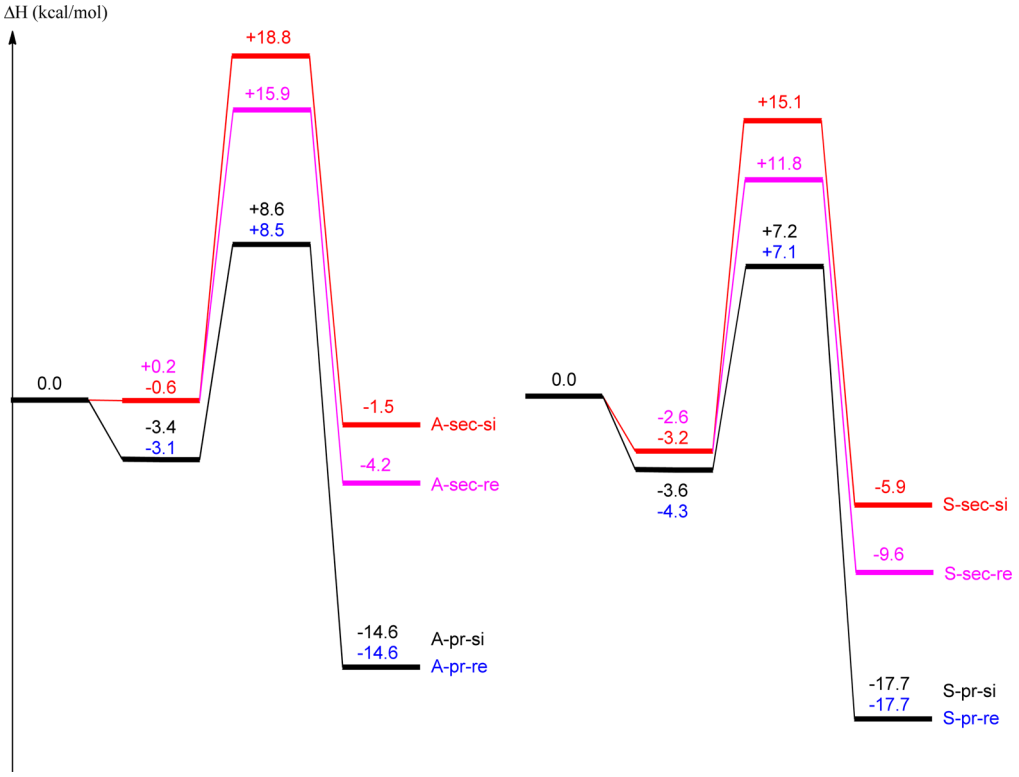

Figure 8. Energetic profiles (calculated with method **B**) of the four types of primary insertion reactions for the *anti* (left) and *syn* (right) configurations of **1***. The zero of energy is, for both profiles, the *anti* configuration of **1*** + propylene molecule on the infinite distance. These energetic data are directly related to Tables 2 and 3

7) for the transition state from the A-pr-*si* structure optimized with the three methods **A**, **B**, and **C**. In fact, the structural parameters did not vary much and the important charges alternation, being typical of [2s+2s] transition states,[26] was found for the three methods.

At a more chemical level, it is noteworthy that A-pr-*re* and A-pr-*si* adducts basically have the same energy profiles, with accessible activation barriers (around +11 kcal/mol) and favorable formation of insertion products (around −10 kcal/mol with respect to the corresponding adducts). On the other hand, the secondary insertions are not competitive because they exhibit higher activation barriers and afford less stable products; this can be seen in a more graphic depiction of the energetic data of Table 2 calculated with method **B** (which leads to the same chemical conclusions as the other methods) in Figure 8. The secondary insertion reactions are less kinetically accessible than the corresponding primary insertion reactions because of steric hindrance. Indeed, the 3D structures of the optimized transition states (Figure 9) show that there is no particular steric repulsion between the methyl group of the propylene molecule and the ligand system in **1*** for the primary insertions. However, for A-sec-*si*, the methyl group points toward the *t*Bu substituent of the Cp, which leads to a steric destabilization of the transition state (by +18.8 kcal/mol with respect to the separated reactants). For A-sec-*re*, the methyl group points toward the *t*Bu of the Flu moiety but the two groups are further apart from each other than for A-sec-*si*, thus, the transition state is slightly lower in energy.

For the four insertion reactions into the *anti* configuration of **1***, the calculations show that the primary insertions are clearly more favorable than the secondary insertions. Moreover, it is again noteworthy that the dispersion effects of GD3BJ (method

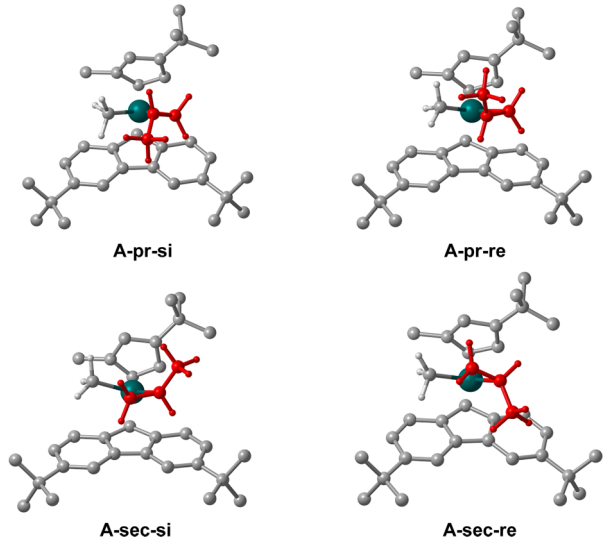

Figure 9. Optimized transition state structures (computed with method **B**) for the four possible insertions of propylene into the *anti* configuration of **1***. For clarity, the hydrogen atoms of the Cp and Flu moieties have been omitted, as well as the entire C(Ph)H bridge. The propylene molecule is depicted in red.

C) overestimate the stabilization of the olefin adducts. Thus, method **B** seems to treat better this zirconocenium system.

Analogously, energetic data of the four possible insertions starting from the *syn* complex were computed via the same four different ways (Table 2). Basically, the same conclusions arise concerning the differential effects of the methods. The solvent and entropy effects tend to shift the energy profiles toward

dx.doi.org/10.1021/cs5016436 | *ACS Catal.* 2015, 5, 416−425

higher values, whereas the dispersion effects tend to shift the energy profiles toward smaller values. Again, the dispersion corrections tend to overstabilize the corresponding adducts (e.g., −16.5 kcal/mol for S-pr-*re*). At a chemical level, the primary insertion reactions are both accessible (around +10 kcal/mol) and yield a stable *iso*-butyl product (around −13 kcal/mol with respect to the adducts). The energy profiles are summarized in Figure 8 for method **B**. At the transition state level, there is no steric repulsion between the propylene molecule and the ligands of **1*** for the primary reactions (Figure 10); on the other hand, the methyl group points

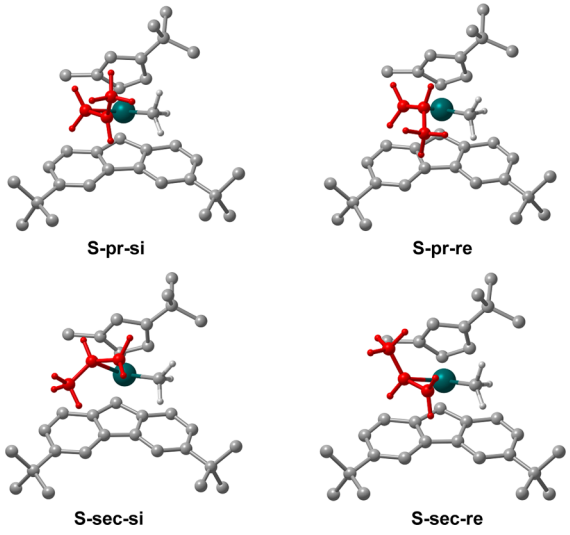

Figure 10. Optimized transition state structures (calculated with method **B**) for the four possible insertions of propylene into the *syn* configuration of **1***. For clarity, the hydrogen of the Cp and Flu moieties have been omitted, as well as the entire C(Ph)H bridge. The propylene molecule is depicted in red.

toward the *t*Bu group of the Flu moiety for S-sec-*si* and toward the Me group of the Cp moiety for S-sec-*re*. These steric hindrances lead to higher activation barriers for the secondary insertions.

Basically, the activation barriers for the four primary insertions (A-pr-*si*, A-pr-*re*, S-pr-*si*, and S-pr-*re*) were all similar (around +7−8 kcal/mol for absolute barriers and +11−12 kcal/mol for relative barriers). However, the *iso*-butyl product formed by S-pr-*si* and S-pr-*re* is more stable than the one formed by A-pr-*si* and A-pr-*re* by 3.1 kcal/mol for method **B** (see Figure 8). This difference is due to the relative position of the *i*Bu group with respect to the *t*Bu of the Cp moiety: *anti* for S-pr-*re* and S-pr-*si* and *syn* for A-pr-*si* and A-pr-*re*. The optimized structures are presented in Figure 11. The *syn* configuration is higher in energy because of a slight steric repulsion of *i*Bu with the *t*Bu group of the Cp ligand (2.09 Å between the two nearest H atoms), as for complex **1***. Moreover, it is noteworthy that a *β*-agostic interaction (between the C−H bond and Zr) appears in both structures.

The insertion reactions of propylene into the *anti* configuration of **1*** have also been computed with method **G** (Table 3). M06 includes dispersion effects, so these results were expected to compare well with those of method **C**. Overall, the values are indeed quite close, and more importantly, chemical interpretations remain the same with method **G**. Accordingly, the most accessible reactions are those yielding the most stable products A-pr-*re* and A-pr-*si* and also have basically the same energy profile. The reaction mediated by A-sec-*si* remains the less favorable, with a high activation barrier around +20 kcal/mol, and offers an unstable product at around 0 kcal/mol with respect to the adduct. These results show that the overestimation of the dispersion correction observed with GD3BJ also appears with the use of M06.

In order to better evidence the differential effects of methods **A**, **B**, and **C**, another type of reactivity was computed. Schematic representations of four main possible C−H activations of propylene are depicted in Figure 12. Activation mode **I** is the allylic activation, where one of the hydrogens of the methyl group of the propylene molecule is transferred to the methyl group of **1*** in order to form an allyl complex with concomitant release of methane. The corresponding transition state structure is a typical *σ*-bond metathesis, with a four-membered cycle. Allylic complexes, due to their high thermodynamic stability, are usually known to stop catalytic polymerization processes by blocking the coordination sites of

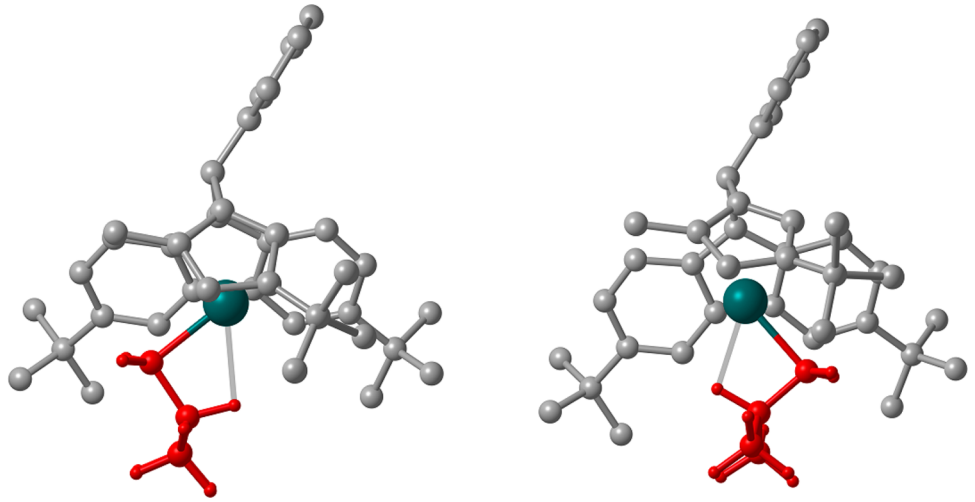

Figure 11. Optimized structures of the two *anti* (left) and *syn* (right) configurations of the *iso*-butyl product. For clarity, the hydrogen atoms of the bridge and the Flu and Cp moieties have been omitted. The *iso*-butyl group is depicted in red.

dx.doi.org/10.1021/cs5016436 | *ACS Catal.* 2015, 5, 416−425

Table 3. Energetic Data (ΔH, kcal/mol) Calculated with Method G for the Insertion Reactions between the *anti* Configuration of 1* and a Propylene Molecule[a]

	A-pr-*re*	A-pr-*si*	A-sec-*re*	A-sec-*si*
adduct	−13.7 (−15.7)	−14.6 (−15.0)	−10.6 (−11.2)	−12.0 (−13.3)
TS	+12.5 (+11.2)	+12.0 (+9.9)	+16.4 (+13.9)	+21.6 (+19.5)
products	−9.1 (−9.5)	−8.3 (−10.2)	−2.7 (−5.7)	+1.2 (−0.8)

[a]The activation energies and the energies of reaction are given with respect to the corresponding adducts. The energetic values (in ΔH) calculated with method **C** are given in parentheses.

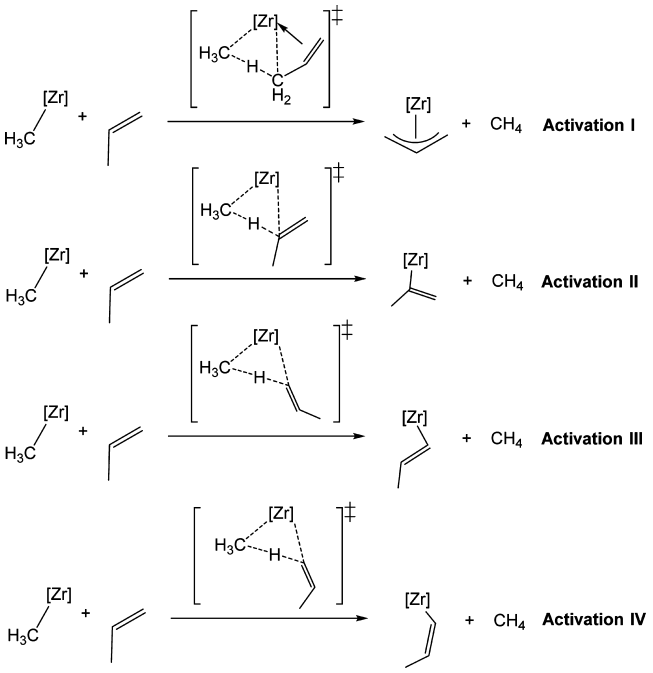

Figure 12. Four possible C−H activation modes of propylene investigated with the *anti* configuration of **1***.

the catalyst. Activation modes **II**, **III**, and **IV** are all processes where one of the vinylic hydrogens of propylene is transferred to the methyl group of **1***. All these processes proceed via σ-bond metathesis transition states.

The differences between methods **A**, **B**, and **C** have also been studied for these C−H activation reactions. Geometrical parameters and NPA charges are presented in Figure 13 for the allylic activation transition states. Basically, there is no geometrical or electronic difference and the charge alternation is the same for the three methods.

The energetic data of the four different C−H activation reactions starting from the complex *anti* were computed via four different ways (Table 4). For activation I, the energies of

Table 4. Energetic Data (kcal/mol) Calculated for C−H Activation Reactions between the *anti* Configuration of 1* and a Propylene Molecule[a]

reaction		ΔH (A)	ΔH (B)	ΔH (C)	ΔG (C)
activation I	adduct	−10.0	−3.4	−15.5	−3.4
	TS	+16.0	+20.5	NC	NC
	products	−14.1	−14.3	−8.2	−21.2
activation II	adduct	−10.4	−4.0	−16.4	−3.2
	TS	+25.6	+29.9	NC	NC
	products	+2.6	+0.1	+6.6	−4.2
activation III	adduct	−6.1	−1.1	−13.8	−0.1
	TS	+17.8	+20.6	+21.0	+19.1
	products	−0.7	−2.9	+7.1	−6.9
activation IV	adduct	−8.9	−2.2	−15.0	−2.4
	TS	+23.2	+24.3	+24.5	+25.3
	products	+5.4	+1.8	+10.4	−0.8

[a]The activation energies and the energies of reaction are given with respect to the corresponding adducts. NC: Not computed because of problems during the frequency calculations.

the propylene adduct follow the same trends as for the insertion reactions. The addition of solvent tends to destabilize the olefin adduct while the addition of dispersion highly stabilizes it. The entropy effect and the dispersion effect completely compensate, since the results with ΔH (**B**) and ΔG (**C**) are exactly the same. The relative activation barriers are quite close for methods **A** and **B** but it was impossible to calculate the values for method **C**. It is also the case for the transition state of activation mode **II**.

In contrast with the insertion reactions, these C−H activation reactions start with two reactants and yield two products. The formation of the two separated products breaks some dispersion stabilizing interactions, which leads to a destabilization of the products with respect to the adducts for ΔH (**C**). On the contrary, the entropy effects tend to stabilize the separated products because of the high disorder formed by the release of the small methane molecule.

The exact same trends were obtained for the three other C−H activation reactions. In this case, for activations III and IV,

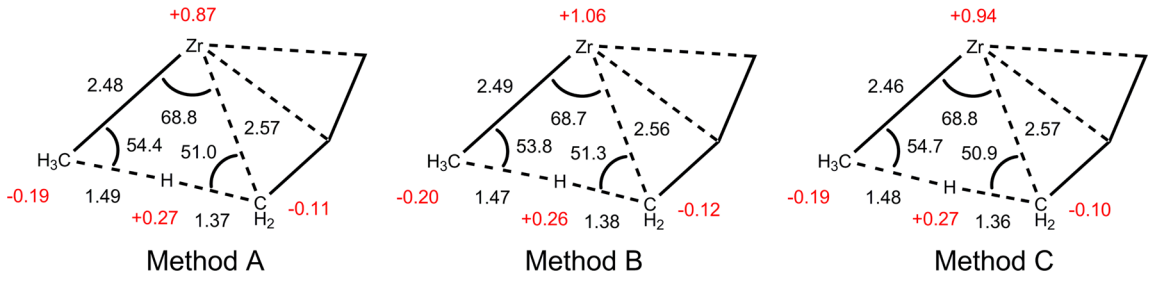

Figure 13. Geometrical parameters and NPA charges computed for the optimized structures of the allylic activation (activation mode **I**) transition state for the three different methods.

dx.doi.org/10.1021/cs5016436 | ACS Catal. 2015, 5, 416−425

the frequency calculations of the transition states worked out and led to relative activation barriers completely equivalent to the ones calculated with methods **A** and **B**. Hence, as for the insertions reactions, it is thus noticeable that the calculated activation barriers for the C−H activation reactions are globally the same for all methods. However, this time, the difference between the methods cannot be summarized by a shift of the energy profiles because energetic differences appear not only for the formation of the olefin adducts but also for the formation of the activation products.

At a chemical level, these activation reactions all present high relative activation barriers (more than 20 kcal/mol for method **B**). Thus, they are not competitive with insertion reactions.

CONCLUSION

The primary insertion of propylene into the yttrium complex **2**, as well as the primary and secondary insertions of propylene into both the *anti* and *syn* configurations of the zirconium complex **1*** were all computed with different methods. Because it is known that an equilibrium between free and bound propylene exist in these types of systems, the stabilization of the olefin adduct with respect to the separated reactants should not be important. On that matter, dispersion effects tend to overestimate the stabilization of the olefin adducts in all cases. For the yttrium system, the best results were obtained when both the solvent and the dispersion effects were taken into account. On the other hand, for the zirconocene system, the best results were obtained when only the solvent effects are included. Indeed the dispersion effects lead to a strong stabilization of olefin adducts (−15 kcal/mol in terms of enthalpy) because of the high steric bulk in **1***. However, when the calculation of entropy was incorporated into the calculation, the effects of dispersion and entropy totally compensated each other. It is important to note that chemical interpretations of the results with and without dispersion corrections remain basically the same. The only effect of the dispersion correction is the shift of the energy profile toward lower energies. However, because the dispersion corrections lengthen the computation time of the optimizations by around 30% and do not compute well ΔH_{coord}, it seems both more correct and more practical to use a method without dispersion effects. In particular, method **B** (that uses B3PW91 in combination with SMD) is a good compromise between the computational cost and the accuracy.

From a chemical perspective, this study shows that the primary insertions of propylene into the Zr−Me bond are more favorable than secondary insertions, both kinetically and thermodynamically; this is a well-known trend in Ziegler−Natta polymerization. The insertions into the *syn* configuration of complex **1*** lead to a more stable *iso*-butyl product than insertions into the *anti* configuration, because of lowered steric repulsions in the former case. The C−H activations of propylene by **1***, which are the deactivation steps of the catalyst, are found to be not favorable kinetically, with high energy barriers of 20 to 30 kcal/mol, and thus not competitive with the insertions reactions of propylene.

ASSOCIATED CONTENT

Supporting Information

The following file is available free of charge on the ACS Publications website at DOI: 10.1021/cs5016436.

Cartesian coordinates of all optimized structures (PDF)

AUTHOR INFORMATION

Corresponding Author

*E-mail: laurent.maron@irsamc.ups-tlse.fr.

Notes

The authors declare no competing financial interest.

ACKNOWLEDGMENTS

This work was gratefully supported by TOTAL SA and TOTAL Research Feluy. L. Maron and L. Castro thank the CALMIP for computation time.

REFERENCES

(1) (a) Resconi, L.; Fritze, C. In *Polypropylene Handbook*; Pasquini, N., Ed.; Hanser Publishers: Munich, 2005; pp 107−147. (b) Kaminsky, W. *Macromolecules* **2012**, *45*, 3289−3297. (c) Fink, G.; Brintzinger, H. H. In *Metal-Catalysis in Industrial Organic Processes*; Chiusoli, G. P., Maitlis, P. M., Eds.; Royal Society of Chemistry: Colchester, 2006; pp 218−254.

(2) For leading reviews, see: (a) Alt, H.; Samuel, E. *Chem. Soc. Rev.* **1998**, 323−329. (b) Alt, H. *Macromol. Chem. Symp.* **2001**, *173*, 65−76. (c) Razavi, A. *Coord. Chem. Rev.* **2006**, *250*, 155−169.

(3) For leading references, see: (a) Ewen, J. A.; Jones, R. L.; Razavi, A.; Ferrara, J. D. *J. Am. Chem. Soc.* **1988**, *110*, 6255−6256. (b) Razavi, A.; Bellia, V.; De Brauwer, Y.; Hortmann, K.; Peters, L.; Sirol, S.; Van Belle, S.; Thewalt, U. *Macromol. Chem. Phys.* **2004**, *205*, 347−356.

(4) Razavi, A.; Bellia, V.; Baekelmans, D.; Slawinsky, M.; Sirol, S.; Peters, L.; Thewalt, U. *Kinet. Catal.* **2006**, *47*, 257−267.

(5) Miller, A.; Bercaw, J. E. *Organometallics* **2002**, *21*, 934−945.

(6) (a) Kirillov, E.; Marquet, N.; Bader, M.; Razavi, A.; Belia, V.; Hampel, F.; Roisnel, T.; Gladysz, J. A.; Carpentier, J.-F. *Organometallics* **2011**, *30*, 263−272. (b) Bader, M.; Marquet, N.; Kirillov, E.; Roisnel, T.; Razavi, A.; Lhost, O.; Carpentier, J.-F. *Organometallics* **2012**, *31*, 8375−8387.

(7) (a) Wondimagegn, T.; Wang, D.; Razavi, A.; Ziegler, T. *Organometallics* **2009**, *28*, 1383−1390. (b) Tomasi, S.; Razavi, A.; Ziegler, T. *Organometallics* **2009**, *28*, 2609−2618.

(8) (a) Tomasi, S.; Razavi, A.; Ziegler, T. *Organometallics* **2007**, *26*, 2024−2036. (b) Wang, D.; Tomasi, S.; Razavi, A.; Ziegler, T. *Organometallics* **2008**, *27*, 2861−2867. (c) Wondimagen, T.; Wang, D.; Razavi, A.; Ziegler, T. *Organometallics* **2008**, *27*, 6434−6439.

(9) (a) Barros, N.; Mountford, P.; Guillaume, S. M.; Maron, L. *Chem.—Eur. J.* **2008**, *14*, 5507−5518. (b) Jenter, J.; Roesky, P. W.; Ajellal, N.; Guillaume, S. M.; Susperregui, N.; Maron, L. *Chem.—Eur. J.* **2010**, *16*, 4629−4638. (c) Dyer, H. E.; Huijser, S.; Susperregui, N.; Bonnet, F.; Schwarz, A. D.; Duchateau, R.; Maron, L.; Mountford, P. *Organometallics* **2010**, *29*, 3602−3621. (d) Fang, J.; Yu, I. S.; Mehrkhodavandi, P.; Maron, L. *Organometallics* **2013**, *32*, 6950−6956. (e) Wang, L. F.; Kefalidis, C. E.; Sinbandhit, S.; Dorcet, V.; Carpentier, J. F.; Maron, L.; Sarazin, Y. *Chem.—Eur. J.* **2013**, *19*, 13463−13478.

(10) (a) Tobisch, S.; Ziegler, T. *J. Am. Chem. Soc.* **2004**, *126*, 9059−9071. (b) Tobisch, S.; Ziegler, T. *Organometallics* **2003**, *22*, 5392−5405. (c) Fan, L. Y.; Harrison, D.; Woo, T. K.; Ziegler, T. *Organometallics* **1995**, *14*, 2018−2026. (d) Woo, T. K.; Fan, L.; Ziegler, T. *Organometallics* **1994**, *13*, 2252−2261. (e) Woo, T. K.; Fan, L.; Ziegler, T. *Organometallics* **1994**, *13*, 432−433. (f) Deng, L. Q.; Margl, P.; Ziegler, T. *J. Am. Chem. Soc.* **1997**, *119*, 1094−1100. (g) Margl, P.; Deng, L. Q.; Ziegler, T. *J. Am. Chem. Soc.* **1999**, *121*, 154−162.

(11) Marenich, A. V.; Cramer, C. J.; Truhlar, D. G. *J. Phys. Chem. B* **2009**, *113*, 6378−6396.

(12) Grimme, S. *J. Comput. Chem.* **2006**, *27*, 1787−1799.

(13) Zhao, Y.; Truhlar, D. G. *Theor. Chem. Acc.* **2008**, *120*, 215−241.

(14) (a) Grimme, S.; Antony, J.; Ehrlich, S.; Krieg, H. *J. Chem. Phys.* **2010**, *132*, 154104−1−154104−19. (b) Grimme, S.; Ehrlich, S.; Goerigk, L. *J. Comput. Chem.* **2011**, *32*, 1456−1465.

(15) (a) Becke, A. D. *J. Chem. Phys.* **1993**, *98*, 5648−5652. (b) Burke, K.; Perdew, J. P.; Yang, W. In *Electronic Density Functional Theory: Recent Progress and New Directions*; Dobson, J. F., Vignale, G., Das, M. P., Eds.; Plenum Press: New York, 1998.
(16) Casey, C. P.; Lee, T. Y.; Tunge, J. A.; Carpenetti, D. W., II *J. Am. Chem. Soc.* **2001**, *123*, 10762−10763.
(17) Frisch, M. J.; Trucks, G. W.; Schlegel, H. B.; Scuseria, G. E.; Robb, M. A.; Cheeseman, J. R.; Scalmani, G.; Barone, V.; Mennucci, B.; Petersson, G. A.; Nakatsuji, H.; Caricato, M.; Li, X.; Hratchian, H. P.; Izmaylov, A. F.; Bloino, J.; Zheng, G.; Sonnenberg, J. L.; Hada, M.; Ehara, M.; Toyota, K.; Fukuda, R.; Hasegawa, J.; Ishida, M.; Nakajima, T.; Honda, Y.; Kitao, O.; Nakai, H.; Vreven, T.; Montgomery, J. A., Jr.; Peralta, J. E.; Ogliaro, F.; Bearpark, M.; Heyd, J. J.; Brothers, E.; Kudin, K. N.; Staroverov, V. N.; Kobayashi, R.; Normand, J.; Raghavachari, K.; Rendell, A.; Burant, J. C.; Iyengar, S. S.; Tomasi, J.; Cossi, M.; Rega, N.; Millam, M. J.; Klene, M.; Knox, J. E.; Cross, J. B.; Bakken, V.; Adamo, C.; Jaramillo, J.; Gomperts, R.; Stratmann, R. E.; Yazyev, O.; Austin, A. J.; Cammi, R.; Pomelli, C.; Ochterski, J. W.; Martin, R. L.; Morokuma, K.; Zakrzewski, V. G.; Voth, G. A.; Salvador, P.; Dannenberg, J. J.; Dapprich, S.; Daniels, A. D.; Farkas, Ö.; Foresman, J. B.; Ortiz, J. V.; Cioslowski, J.; Fox, D. J. *Gaussian 09*, revision D.01; Gaussian, Inc.: Wallingford, CT, 2009.
(18) (a) Andrae, D.; Haeussermann, U.; Dolg, M.; Stoll, H.; Preuss, H. *Theor. Chim. Acta* **1990**, *77*, 123−141. (b) Martin, J. M. L.; Sundermann, A. *J. Chem. Phys.* **2001**, *114*, 3408−3420.
(19) Hehre, W. J.; Ditchfield, R.; Pople, J. A. *J. Chem. Phys.* **1972**, *56*, 2257−2261.
(20) Watson, L.; Eisenstein, O. *J. Chem. Educ.* **2002**, *79*, 1269−1277.
(21) Reed, A. E.; Curtiss, L. A.; Weinhold, F. *Chem. Rev.* **1988**, *88*, 899−926.
(22) (a) Watson, P. L.; Parshall, G. W. *Acc. Chem. Res.* **1985**, *18*, 51−56. (b) Watson, P. L. *J. Am. Chem. Soc.* **1982**, *104*, 337−339. (c) Watson, P. L.; Roe, D. C. *J. Am. Chem. Soc.* **1982**, *104*, 6471−6473.
(23) (a) Schultz, N. E.; Zhao, Y.; Truhlar, D. G. *J. Comput. Chem.* **2008**, *29*, 185−189. (b) Zhao, Y.; Truhlar, D. G. *Acc. Chem. Res.* **2008**, *41*, 157−167.
(24) Weymuth, T.; Couzijn, E. P. A.; Chen, P.; Reiher, M. *J. Chem. Theory Comput.h* **2014**, *10*, 3092−3103.
(25) Kefalidis, C. E.; Stasch, A.; Jones, C.; Maron, L. *Chem. Commun.* **2014**, *50*, 12318−12321.
(26) Steigerwald, M. L.; Goddard, W. A., III *J. Am. Chem. Soc.* **1984**, *106*, 308−311.